Polarimetry with EMIR/XPOL
Commissioning report (project T04-09)

Helmut Wiesemeyer[1] **& Clemens Thum**
IRAM
10 August 2010

Summary. Following the installation of the new EMIR receiver in spring 2009, the XPOL observing mode needed to be adapted and the consequences for polarization observations to be investigated. Here we report on test measurements made at 90 and 230 GHz. XPOL now works at these EMIR bands with lower on–axis instrumental polarization than before. Sidelobe levels are however not significantly reduced, with the consequence that observations of extended sources still demand special care. Commissioning of XPOL in the E150 and E330 bands remains to be done.

1 What is new with EMIR

EMIR and its associated warm optics present several differences compared to the previous generation of ABCD receivers which have direct relevance to polarization observations. Firstly and most importantly, all eight mixers of EMIR are located in one single dewar. The polarization splitting wire grids of all four frequency bands are also inside this dewar. The beneficial consequence of this higher level of integration (previously, different polarizations were housed in different dewars) is that any alignment variations between the horizontal and vertical beams are negligible as long as the dewar remains cold.

The second difference concerns the phase measurement. As before, the phase between the receivers is derived from the difference signal between hot and ambient loads where a wire grid is introduced in front of the cold load. The warm optics of EMIR which redirects the beams from the feeds back into the dewar toward internal cold loads, did however not provide sufficient space for the introduction of a wire gird. For polarization calibration (temperature and phase) an external cold load (LN_2) has been set up. Its effective temperature must be introduced into paKo by the observer. The precision of the phase calibration is not affected by this change.

The third difference concerns the generation of the local oscillator signal. Both polarizations now obtain their LO signal from the same Gunn oscillator and multiplier (if applicable). The same is true for the first downconversion. This greatly reduces the phase noise compared to the previous receivers where each polarization had its own Gunn oscillator (and multiplier).

The last important difference concerns the optical paths. The internally combined vertical and horizontal beams of the four frequency bands leave the dewar through four different windows.The warm EMIR optics then folds these beams back onto the positions of the 3mm (or the 2mm) window. The telescope optical axis was chosen to be located midway between the 3 and 2mm windows. Some asymmetry is thus introduced into the optical properties of each receiver band.

We have investigated the implications of these differences in several technical sessions (June 2009, April 2010, June 2010) where we concentrated on the 90 and 230 GHz bands. No tests were made yet at 150 and 330 GHz. A detailed description of XPOL with the previous receivers ABCD is given by Thum et al. (2008).

2 Alignment

The alignment of the pointing axes between horizontal (H) and vertical (V) polarizations has been investigated in all test sessions and found to be better than 1" at 90 and 230 GHz. At this level, no variations with time were detected.

[1] on sabbatical leave at MPIfR

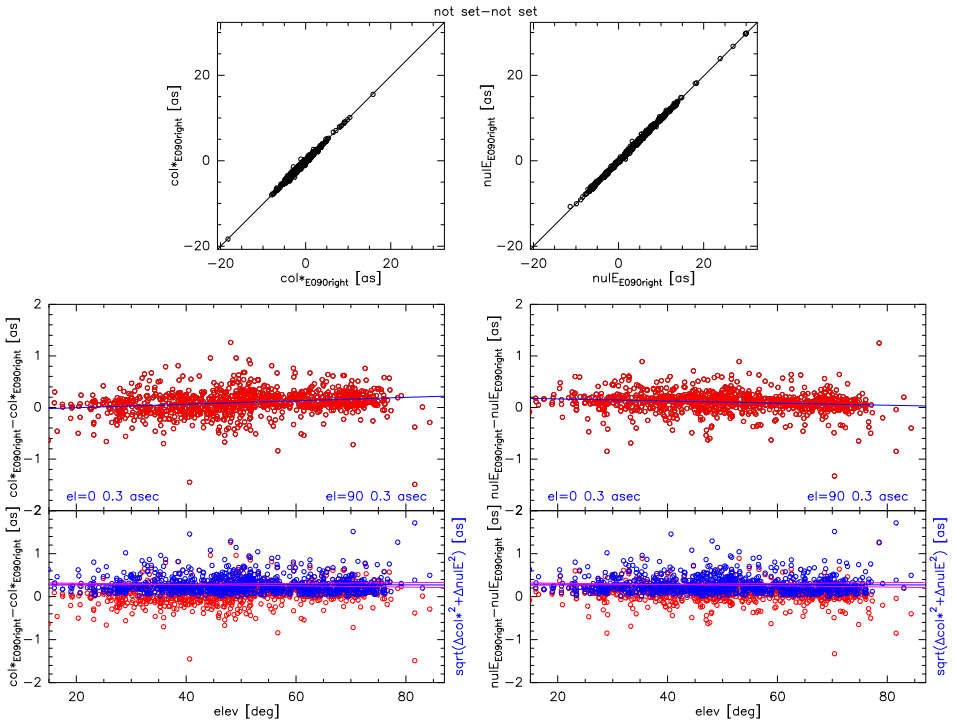

Figure 1: Alignment difference between polarizations, H−V, of the EMIR 90 GHz band. Top panels: Azm (left) and Elv (right) collimation errors of H vs. those of V during the ≈ 1.5 years after installation of EMIR. Lower panels: Azm (left) and Elv (right) collimation errors of H−V vs. elevation (red). The blue points are the quadratically combined sum of the Azm and Elv errors (*courtesy:* R. Zylka).

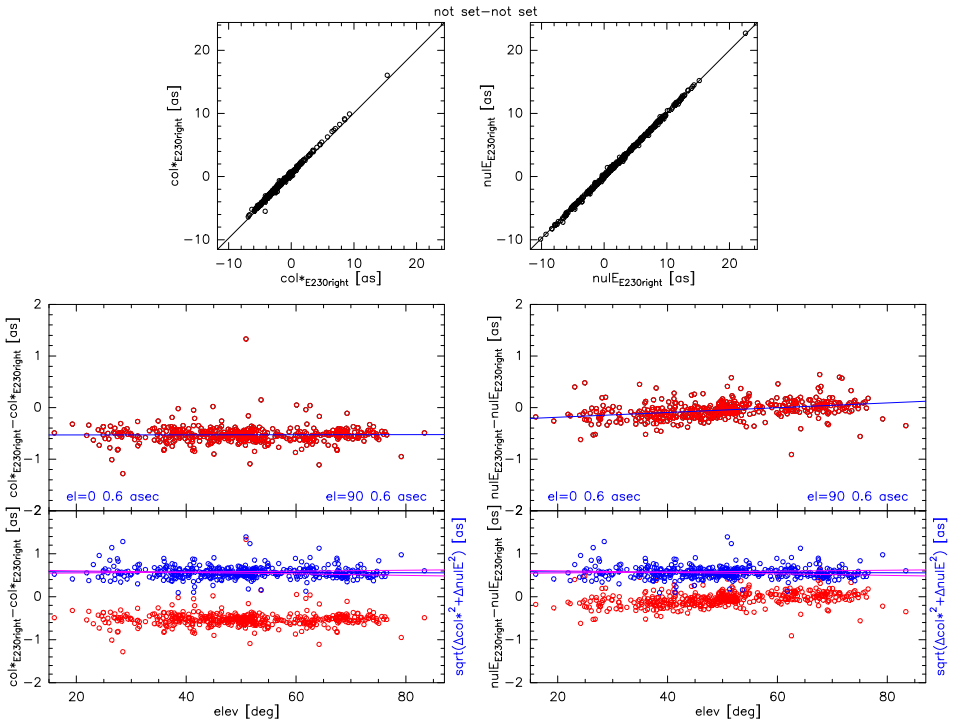

Figure 2: Same as Fig. 1, but for the 230 GHz band (*courtesy:* R. Zylka).

Exploiting the much larger data base available from pointing observations made since the installation of EMIR (April 2009) until present (June 2010), a much higher accuracy can be achieved. Using the MOPSIC monitor and retaining only pointings of good quality (R. Zylka, priv. comm.), the misalignment H-V was found to be barely detectable at 90 GHz and small at 230 GHz (Tab. 1). Figs. 1 and 2 show this data, also plotted against elevation. The rotation due to the location of the receivers in the Nasmyth focus is apparent.

Table 1: Alignment, in arcsec, between EMIR horizontal (H) and vertical (V) polarization beams as derived from 1.5 years of pointing observations.

band	H−V
90 Ghz	$+0.1 \pm 0.1$
230 GHz	-0.5 ± 0.1

Maps of the Stokes beams

2009 session

Beam maps from June (Fig. 3) show that the on–axis instrumental polarizations in Stokes I, Q, U and V qualitatively (and roughly quantitatively) correspond to those obtained with the A100/B100 receivers after a realignment session. The bipolar pattern in Stokes V is owing to small differences of the illumination of the subreflector by the orthogonally polarized horns. The (x,y) coordinates illustrate the projection of the Nasmyth horizontal and vertical directions on to the sky.

Despite the better alignment of EMIR with respect to that of the old cryostats, resulting in a lower instrumental polarization on the pointing axis, the levels of the polarized sidelobes remain high. Moreover, the patterns, when projected onto the sky, do not show anymore the simple rotation with the angle χ_0 as with the previous receivers [2]. This departure from a simple symmetry will be seen to be even stronger at λ 1.3 mm.

2010 session

Two beam maps of Venus (Figs. 4 and 5) were obtained on April 28, each consisting of two coverages with orthogonal scanning directions. The orientation of the Nasmyth coordinate system as projected onto the sky was only slightly different ($5\overset{\circ}{.}2$ difference between the respective χ_0). The second map (Fig. 5) differs from the first one as it is slightly larger, allowing us to remove a linear spatial baseline from the on-the-fly subscans instead of using dedicated off-source total power measurements. Here both methods yield similar results in Stokes I and Stokes Q, which are sensitive to total power fluctuations. Strangely, Stokes U and V, much less affected by such fluctuations, do show significant differences, e.g. upon comparison of their symmetry properties with respect to the Nasmyth coordinate frame. The mean elevation of both maps differs by $10\overset{\circ}{.}3$ - this suggests that the rotation of sidelobes with elevation is more complex than with the previous receivers (where the sidelobe pattern simply rotated by the angle χ_0 about the the origin of the (x,y) system), possibly due to the off–axis installation of EMIR (Sect. 1).

3 Phase calibration device

As described in sect. 1, XPOL uses external loads for temperature and phase calibration. A measurement for temperature and phase calibration (`cal /grid`) takes about 42 sec, instead of 25 sec for a standard temperature calibration using the internal loads. This increase is mainly

[2] For both EMIR and the A100/B100 receivers, we denote the position angle of the vertical axis of the Nasmyth frame with respect to North as χ_0. With the elevation ϵ and the parallactic angle η we have in a left–reflecting Nasmyth system $\chi_0 = \epsilon - \eta$.

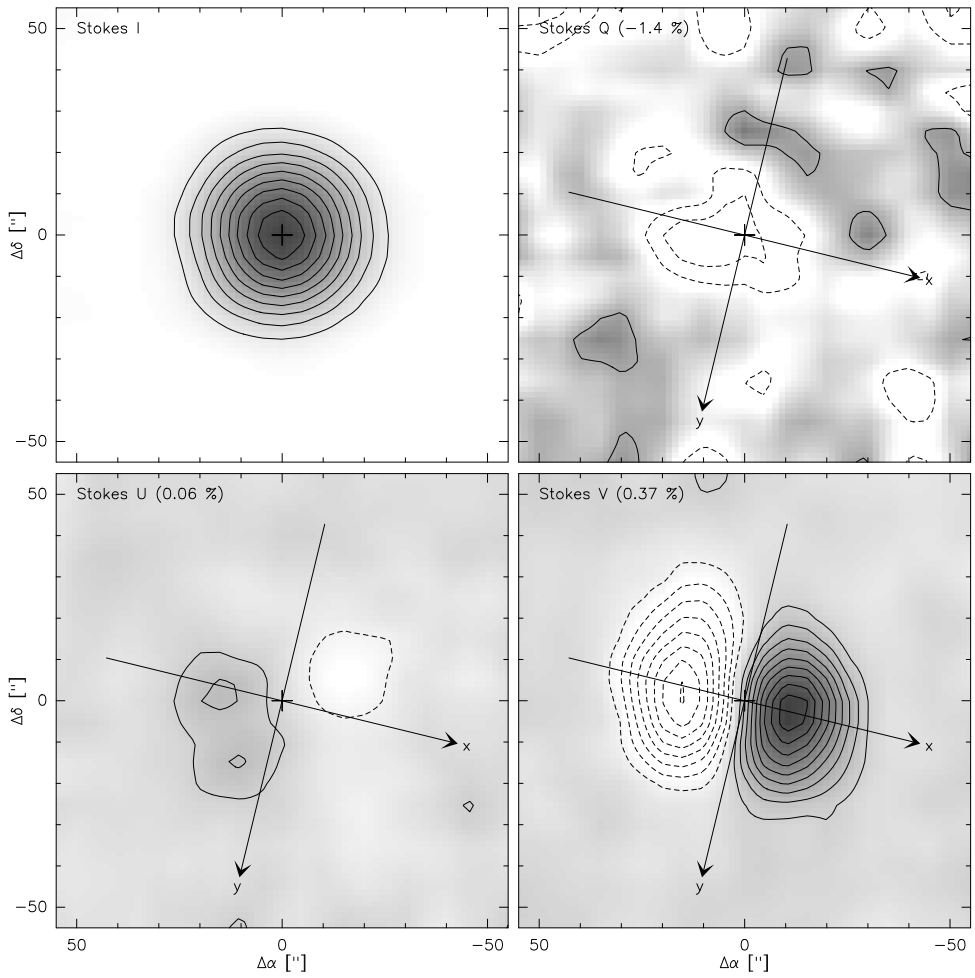

Figure 3: Stokes beam maps at 86.243 GHz taken towards Mars on 2009 June 20 with E090LI. Stokes I (top left, 10% contours, peak temperature 3.38 K $T_{\rm A}^*$), Stokes Q (top right, contour levels at $-40, -20, +20$ mK), Stokes U (bottom left, contour levels $-6, +6, +12$ mK, Stokes V (bottom right, contour levels -48 to -6 mK, 6 mK to 54 mK in steps of 6 mK, zero contour omitted). The values behind the Stokes labels indicate the fractional instrumental polarization (%) at the maximum of the Stokes I image (marked by a cross).

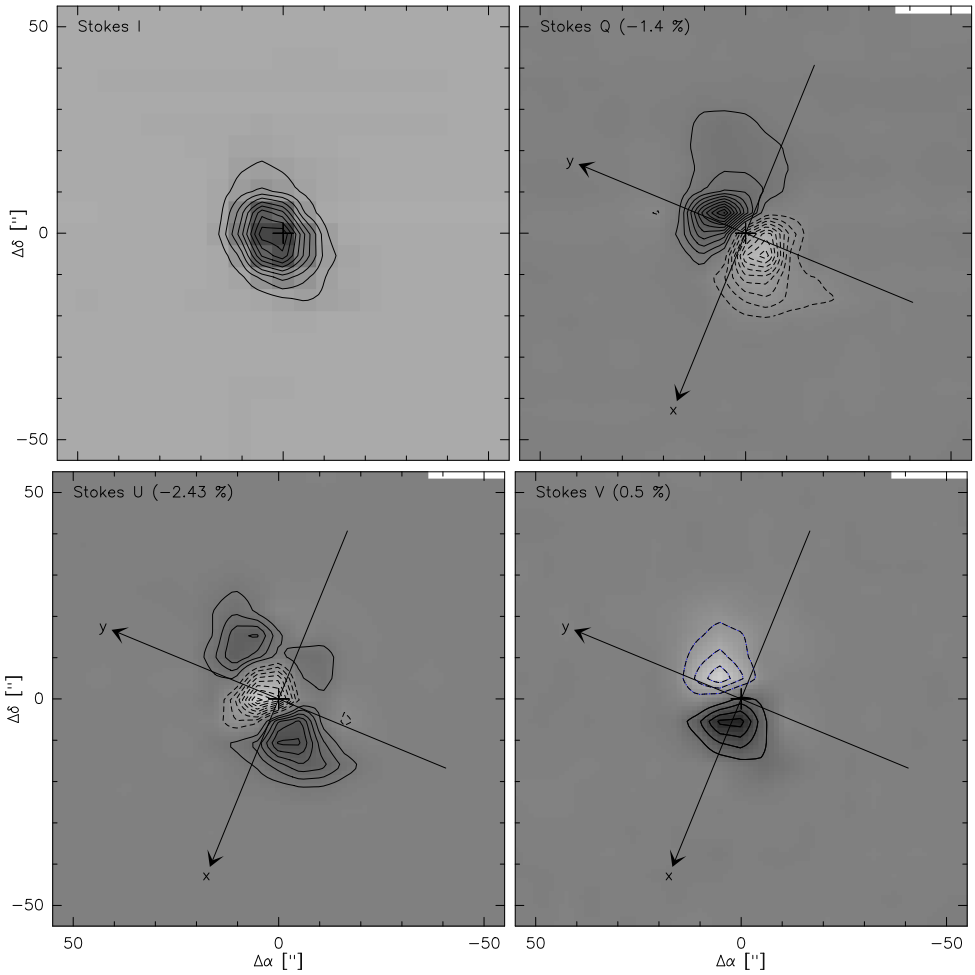

Figure 4: Stokes beam maps taken towards Venus on 2010 April 28 at 231.9 GHz. Stokes I (top left, 10% contours, peak temperature 61.6 K T_A^*), Stokes Q (top right, contour levels from -1.8 to 2.2 K and in steps of 0.2 K, zero contour omitted), Stokes U (bottom left, contour levels −1.8 to +1.2 K in steps of 0.2 K (zero contour omitted), Stokes V (bottom right, contour levels −0.6 to +0.8 K in steps of 0.2 K, without zero contour). The values behind the Stokes labels indicate the fractional instrumental polarization (%) at the maximum of the Stokes I image (marked by a cross).

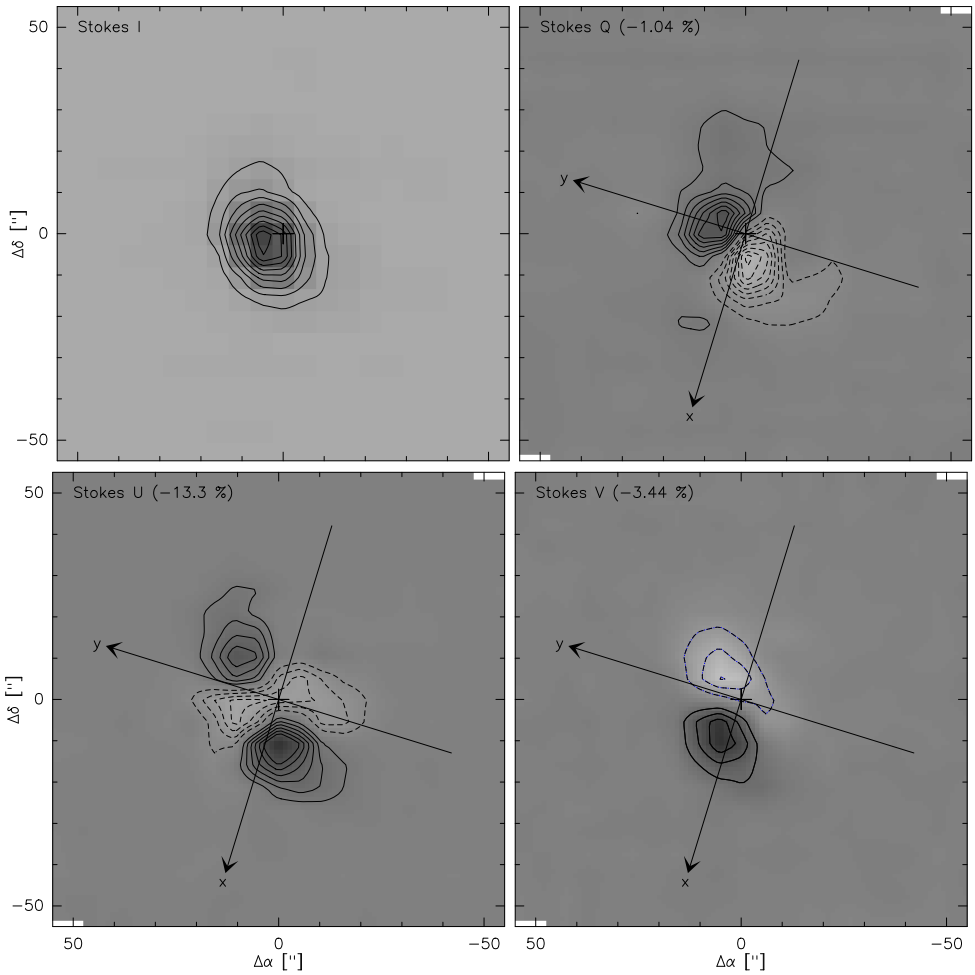

Figure 5: Same as Fig. 4, but taken one hour later and without separate measurements of the off-source atmospheric reference level (the map is slightly larger, therefore from each OTF subscan a spatial linear baseline could be subtracted.)

owing to a time lag of $\simeq 10$ sec between the measurement of the hot load and that of the cold load, and between the LN_2 cold load and grid subscans. Note that a sufficient level of LN_2 must be maintained in its bucket.

Following a suspicion of an elevated loss of cross correlation amplitude in measurements with the phase calibration unit (with respect to observations on the sky), we replaced an undersized grid (i.e., not filling the beam) with a larger one on 2009 August 19. Its position angle, as determined from Stokes Q and $U = \sqrt{I^2 - Q^2}$ (i.e. from total power measurements, assuming zero Stokes V) is 126°, i.e., the same angle as for our polarimetry with the AB cryostats (the value for the grid used in June, July and until August 18 was rather at an angle of 128°). The factor to correct the complex cross correlation for the flux loss due to phase noise was 1.2 with the larger grid, smaller than the one obtained with the undersized grid (1.4), but still too large to be consistent with maser observations on the sky that rather suggest that no such loss exists (see below).

There is a standing wave in the Stokes I and Q spectra, in the on-off measurement between the ambient load and the cold load & grid (of a period of ~ 88 MHz, corresponding to a 170 cm path, which is the distance from EMIR to the external cold load), with a peak-to-peak amplitude of ≈ 3 % of that of the Hot–Cold signal (Fig. 6, left). With the grid used between 2009 June 17 and August 18 the standing wave had a similar period, indicating that the undersized grid did in fact not truncate the beam. For comparison, the ripple in the old system had a period of about 29 MHz and was stronger by a factor of ~ 7 (Fig. 6 right, see also Thum et al., 2008).

4 Phase stability and noise

While it has been ascertained independently that there is no correlated flux loss η in excess of 1 % due to phase noise and confirmed by observations of SiO masers in TX Cam (2009 June 19, Fig. 8), we have to understand where the discrepancy between these estimates and the one derived from the phase calibration comes from. For the latter, we use

$$\eta = \frac{\sqrt{\Re(\mathrm{CC})^2 + \Im(\mathrm{CC})^2}}{\sqrt{I^2 - Q^2}} \tag{1}$$

assuming that the grid is 100 % efficient and that there is no circular polarization. $\Re$(CC) and $\Im$(CC) are the real and imaginary part of the complex cross correlation between the horizontally and vertically polarized receivers, respectively.

A circular regression of the data shown in Fig. 8 (right, Stokes Q vs. Stokes U in Nasmyth reference, integrated across a velocity range with roughly constant polarization properties) yields an instrumental polarization of $(Q, U) = (-0.42, +0.42)$ % (the astronomical fractional linear polarization is given by the radius of the fitted circle, $p_\mathrm{L} = 46.1$ %). The slight ellipticity suggested by the fit in Fig. 8 (left, using individual spectral channels) is neglected by the circular regression. The fitted instrumental polarization in Stokes Q is of the expected order of magnitude (cf. Fig. 3), but that in Stokes U is larger. This may be another indication that the variation of Stokes (Q, U) in the reference frame as a function of elevation and parallactic angle is more complicated than previously assumed.

As a next step yet to be done, the analysis will have to correct the van Fleck correction for the case of a strong polarized signal, hence correlation, and the circular regression will be replaced by a more involved, elliptical one. A test similar to that shown in Fig. 8 still has to be done for the other EMIR bands. Such measurements need extremely stable weather conditions, and the number of useable sources is quite restricted, too.

The phase drift of the XPOL mode is small, about 1°/h, see Fig. 9). The peak–peak phase noise is lower than 1°, the measurement accuracy. The slow drift allows us to calibrate phases together with a temperature calibration, i.e., every 5 to 15 minutes. Both the better phase stability of EMIR/XPOL and the lower phase noise level are a direct consequence of the more integrated design of EMIR.

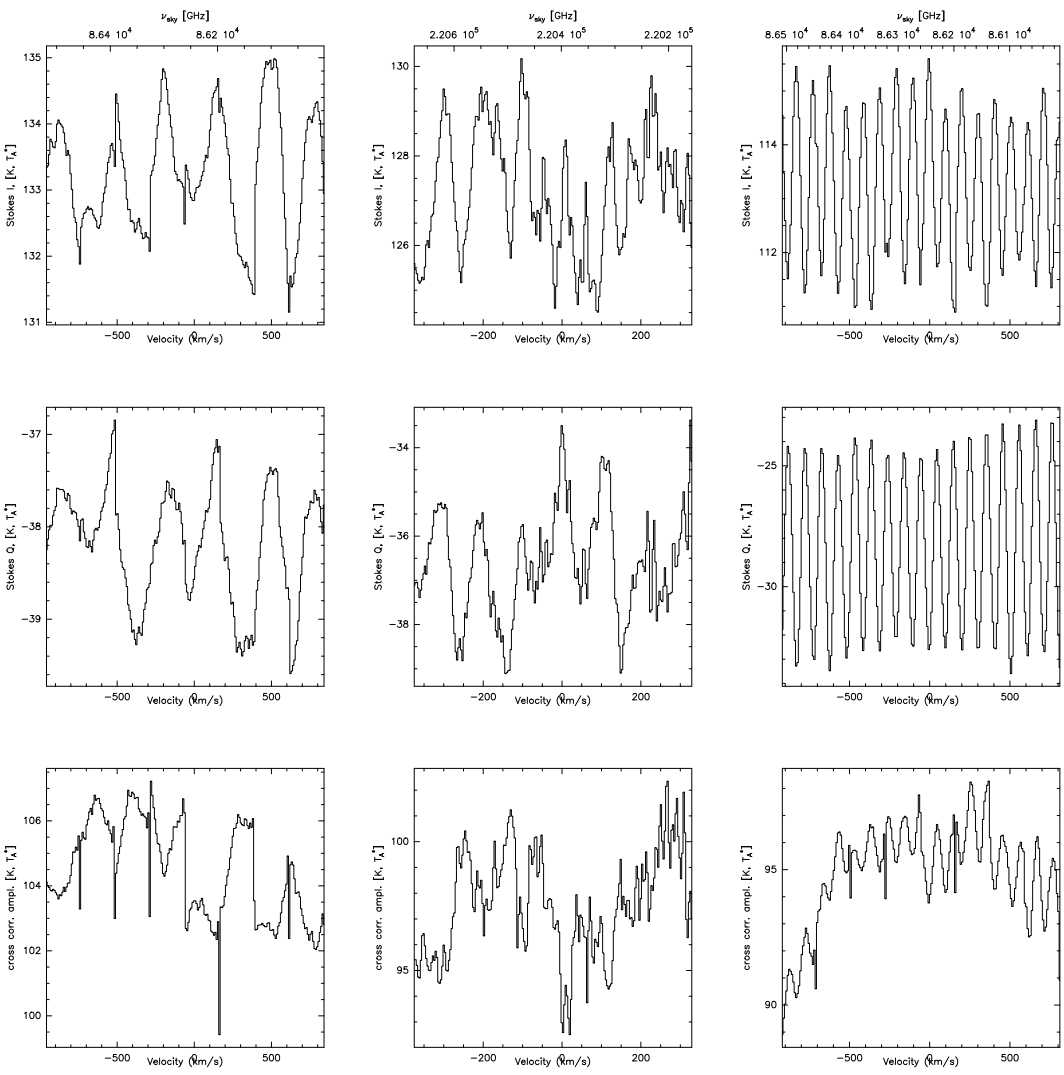

Figure 6: From top to bottom: Stokes I, Q and the cross correlation amplitude vs. channel number, for EMIR grid calibration data from August 2009 (left column, band E090) and June 2009 (middle column, band E230) and for A100/B100 data from 2009 February 20 (right column). The VESPA/XPOL modus in all cases was 640/2.5 (nominal bandwidth/channel spacing, in MHz). The actual bandwidth was 520 MHz (EMIR) and 500 MHz (A100/B100), respectively.

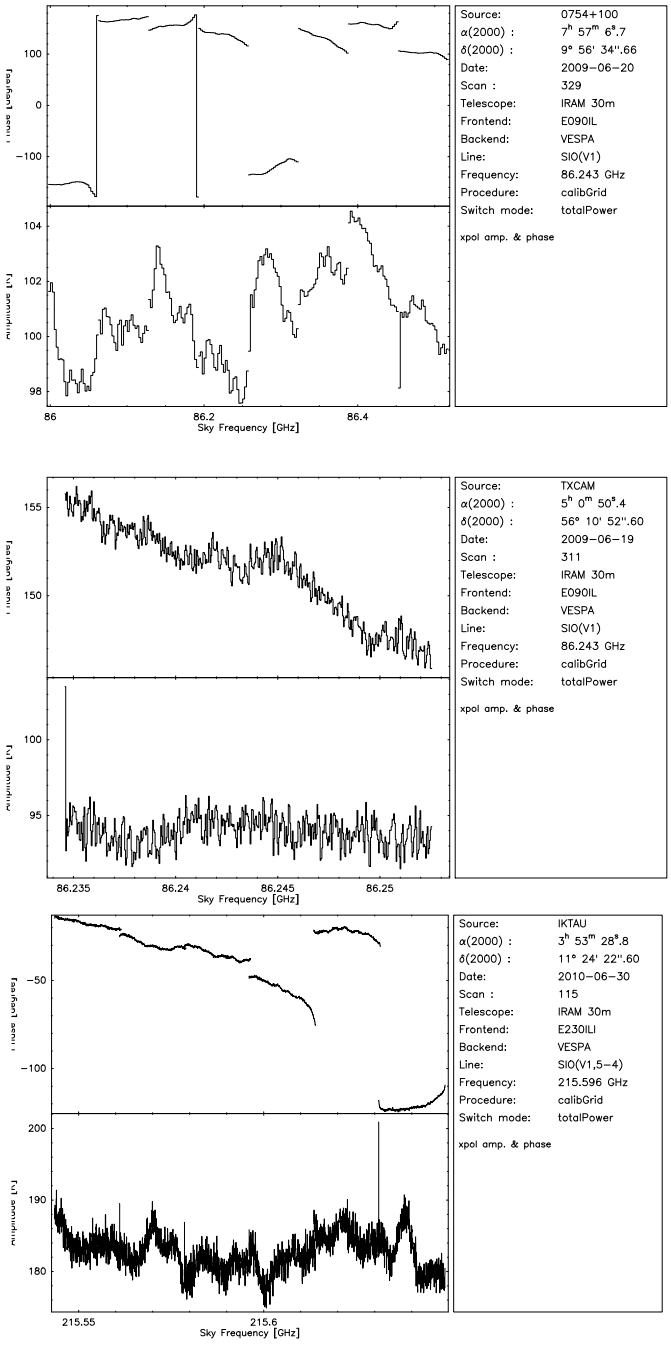

Figure 7: Cross correlation phase and amplitude towards the polarized calibration signal. Top: VESPA/XPOL broad band mode (nominal 640/2.5 MHz bandwidth/channel spacing). The basebands are clearly distinguishable thanks to their different phase characteristics. 2π phase jumps are trivial. Middle: same for the combination 20 MHz/40 kHz. Only one VESPA baseband is needed. Bottom: same for E2 band at 215.6 GHz (XPOL mode 120 MHz/40 kHz, 6 basebands).

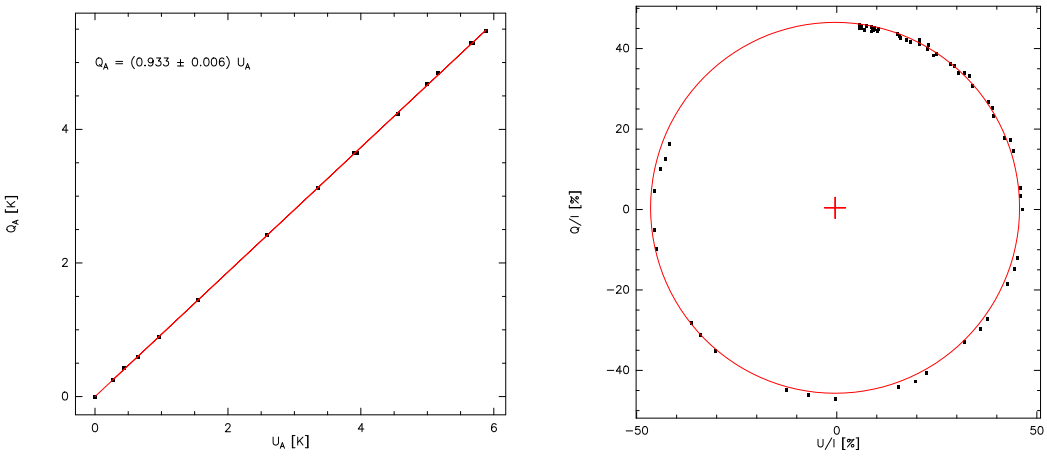

Figure 8: Two representations of Stokes measurements of TX Cam in the Nasmyth reference system. Right: Stokes Q vs. Stokes U (% fractional polarizations of the average signal within the interval from $v_{\rm lsr} = 9.5$ to 11.5 km s^{-1} (where the polarization angle is sufficiently flat). Each dot corresponds to an individual scan. The fit by the circular regression and the fitted center (i.e., instrumental polarization) are shown in red. Left: amplitudes of the sinewaves (function of elevation − parallactic angle) of Stokes Q vs. those of Stokes U. Each dot corresponds to an individual spectral channel. There is no loss in the cross correlation signal (the fit rather suggests the inverse case, since the slope is slightly < 1, this may be a bias owing to the sensitivity of Stokes Q to total power fluctuations).

5 Software

For the XPOL modus of VESPA where two separate spectral bands are used

```
VESPA 1 0.04 40, VESPA 2 0.04 80
```

(part, channel spacing and nominal bandwidth [MHz]), a few upgrades had to be made within Mira during tests on 2009 August 20. The mode is used for Zeeman measurements of CN hyperfine structure and is fully functional now (the modifications are in Gildas version `gag_dev` on `mrt-lx3`, download from `http://www.iram.fr/IRAMFR/GILDAS/`). Furthermore, the sign of Stokes U (Nasmyth) at a zero crossing of Stokes V had to be changed in order to reproduce the known polarization angles of 3C286 and the Crab nebula (see next section).

An updated version of the XPOL widgets for the CLASS software is now available at the telescope on `mrt-lx3` under version `gag_dev`. It is planned to make the xpol widgets for CLASS available via the GILDAS distribution by fall 2010.

6 Astronomical polarization angle verifications

The Crab nebula and 3C286 were observed repeatedly on 2009 June 20 and 31 and on August 20, and several other AGN (1657-261, 1413+135 and 1354+195) on 2009 August 19. Some relevant parameters are summarized in Tabs. 2 and 3. The polarization angles were made consistent by taking the sign of Stokes U at the zero crossing of Stokes V (i.e., after phase calibration) inverted with respect to the A/B 100 receivers, most likely because there the number of reflections is different.

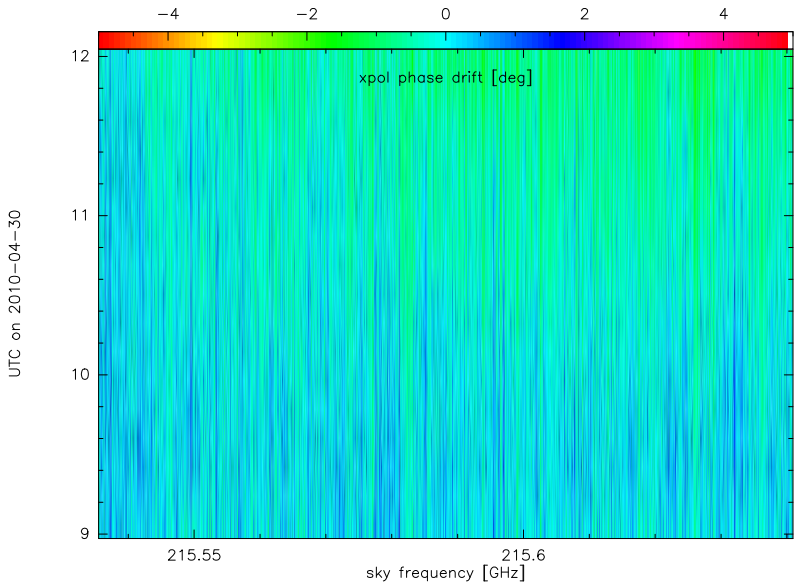

Figure 9: Demonstration of the phase stability of EMIR/XPOL for the high-spectral resolution mode, at the SiO($v1, J = 5 - 4$) frequency observed on 2010 April 30 (measured XPOl phase vs. frequency and time).

Table 2: Polarization measurements of the Crab nebula (CRAB XPOL position, Stokes Q and U are for the Nasmyth reference system).

Date	Q [K]	U [K]	$p_{\rm L}$ [%]	$p_{\rm C}$ [%]	χ [°]	Notes
2009 February 16 (1)	0.139	0.105	21.4	-0.6	142.5	(1)
2009 June 20	0.15	−0.10	18.2	0.1	148.7	(2)
2009 July 31	0.14	0.13	20.4	0.7	146.9	(2)
2009 August 20	0.17	0.21	28.1	1.0	151.2	(2)
2009 Jan 9 – 12	—	—	28.4	<0.1	153.3	(3)

Notes: (1) with A100/B100 receiver, (2) observed with several arcsec of anomalous refraction, (3) Aumont et al. (2009), best current reference. Maps taken at many different χ_0, therefore Stokes Q and U (Nasmyth) are undefined. The upper limit for $p_{\rm C}$ is from Wiesemeyer et al. (2010), after correction for instrumental artefacts.

Table 3: Same with 3C286

Date	Q [mK]	U [mK]	$p_{\rm L}$	$p_{\rm C}$	χ	Notes
2008 December 20(1)	−9	−0.018	14.2	−0.2	36.1	(1)
2009 June 19	−21	5	15.8	−1.1	41.2	(2)
2009 July 31	15	−13	14.5	−0.6	36.5	(2)
2009 August 19	5	−18	13.7	−1.4	35.9	(2)
2009 August 20	−12	4	12.5	0.7	38.9	(2)
2006 October	–	–	13.4	< 0.45	39.6	(3)

Notes: (1) with A100/B100 receiver, (2) unstable weather conditions (anomalous refraction of several arc sec), (3) from Agudo et al. (2010, best current reference).

Table 4: Polarimetry with the ABCD receivers and EMIR - a comparison

	ABCD	EMIR
phase calibration	external (grid in front of compressor cold load)	external (grid in front of LN cold load)
local oscillator	separate for H and V, using a common reference	same LO for H and V
receiver alignment		
absolut[(1)]	variable in time	variable in time
relative[(2)]	variable in time	stable ($0\farcs2$)
correlation loss[(3)]	$\sim 10\%$	insignificant
XPOL spectra and Stokes parameters[(4)]:		
Stokes I	H+V	H+V
Stokes Q	H-V	H-V
Stokes U[(4)]	$-\mathcal{R}\{\mathrm{CC}\}$	$+\mathcal{R}\{\mathrm{CC}\}$
Stokes V[(4)]	$+\mathcal{I}\{\mathrm{CC}\}$	tbd

Notes: (1) receiver alignment with respect to the optical axis, (2) alignment of the horizontally polarized horn with respect to the vertically polarized one, (3) presumably due to phase noise (confirmed by observations of SiO maser polarization), (4) H and V denote the horizontally and vertically polarized brightness, respectively, CC denotes the complex xpol cross correlation after phase calibration. The different signs of Stokes U in the real part of the complex cross correlation (i.e., in the Nasmyth reference frame) are corrected in the data processing.

Acknowledgements

We thank Santiago Navarro for his help with replacing the phase calibration grid by a larger one, and for confirming that there is indeed no excess phase noise in the signal chain, and finding also confirmed by Gabriel Paubert.

References

Agudo, I., Thum, C., Wiesemeyer, H., & Krichbaum, T. P. 2010, ApJS, 189, 1
Aumont, J., et al. 2010, Astron.Astrophys., 514, A70
Thum, C., Wiesemeyer, H., Paubert, G., Navarro, S., & Morris, D. 2008, Publ.Astr.Soc.Pacific, 120, 777
Wiesemeyer, H., Thum, C., & Morris, D. et al., 2010, in preparation

Appendix

PaKo procedures for XPOL setup

In order to avoid the losses owing to the dichroic beam splitters, and also their possible impact on instrumental polarization, we recommend to use only one EMIR band at a time. So far the E090 and E230 bands have been commissioned. For polarimetry, both polarizations of a given EMIR band have to be connected to the same subband (in this example: LI). The cold load temperature has to be set to 77 K, because a liquid nitrogen bath is used as a cold load, and, equipped with a grid, as polarizer for phase calibration.

As an example, a setup for the $\lambda 3$ mm and $\lambda 1$ mm SiO($v1$) maser is given:

```
receiver E0 SiO(v1,2-1) 86.243350  LI /horizontal LI /vertical LI -
                                       /tempload 77 L /eff 0.95 0.95
```

or

```
receiver E2 SiO(V1,5-4) 215.596068 LI /horizontal LI /vertical LI -
                                       /tempload 77 L /eff 0.91 0.91
```

with the corresponding backend setups (at maximum spectral resolution)

```
backend VESPA 1 0.04 20 /receiver e0 h li /mode polar
```

respectively

```
backend VESPA 1 0.04 20 /receiver e2 h li /mode polar
```

Further available combinations of nomincal bandwidth/channel spacing are
80 kHz/240 MHz and 320 kHz/480 MHz. For continuum measurements (AGN monitoring, polarization calibrators) the XPOL mode providing the largest bandwidth is, for the inner subbands,

```
backend VESPA 1 2.5 640 freqoff /receiver e0 h subband /mode polar
```

In this XPOL mode, frequency offsets are needed, with

```
 16.2 < freqoff [MHz] < 38.2
```

for `subband = LI` and `subband = UO`, otherwise

```
 -38.2 < freqoff [MHz] < -16.2
```

All these VESPA setups yield instantaneously four CLASS spectra, namely the horizontal and vertical polarization in the Nasmyth reference system, and the real and imaginary part of the complex cross correlation. It is possible to split VESPA into two parts, yielding four spectra each, e.g., for measurements of the two groups of CN($1-0$) hyperfine components:

```
receiver E2 CN(1-0)113.34 UI /horizontal UI /vertical UI
```

with the corresponding VESPA setup

```
backend VESPA 1 0.04 40 +158.0 /receiver e0 h ui /mode polar
backend VESPA 2 0.04 80 -172.0 /receiver e0 h ui /mode polar
```

Please note that the bandwidth ratio of the two VESPA parts needs to be 2:1 if they are connected to the same EMIR band. This restriction does not hold anymore if the observer plans dual-frequency band observations (with the caveat regarding the dichroic losses in mind).

The XPOL observations then follow the usual observing procedures, except that for each calibration, a subscan on the calibration grid has to be taken, i.e., the syntax for calibrations becomes:

```
calibrate /ambient /cold /grid /sky -600 0
```

etc.
Due to the good phase stability, there is no need to do more calibrations than in non-polarimetric mode.